JOURNAL OF GEOPHYSICAL RESEARCH, VOL. 112, B04301, doi:10.1029/2005JB004056, 2007

Click Here for Full Article

Continuum mathematical modeling of slip weakening in geological systems

Ronaldo I. Borja[1] and Craig D. Foster[1]

Received 16 September 2005; revised 4 April 2006; accepted 18 October 2006; published 5 April 2007.

[1] We describe a framework for mathematical modeling of slip weakening in an initially intact rock mass due to shear strain localization along any arbitrary slip plane. The modeling technique considered is based on continuum mechanics and may be cast directly into a standard nonlinear finite element algorithm for the analysis of prefailure and postfailure responses of geological systems in a boundary value problem. The prefailure behavior is represented by a continuum constitutive model; the postfailure behavior is characterized by frictional yielding on a slip surface with state- and velocity-dependent coefficient of friction. In the context of finite element analysis, slip planes are represented by an embedded strong discontinuity introduced into an initially intact finite element to signal the beginning of postfailure behavior. This paper focuses on the narrow time interval of slip weakening, from the moment the strong discontinuity has been embedded into a finite element until the relative slip has grown to a large enough value for the coefficient of friction to reach steady state. To this end, we formulate a linear slip weakening constitutive law in which the weakening component decays to zero at the same time that the frictional component increases to its value at residual state.

Citation: Borja, R. I., and C. D. Foster (2007), Continuum mathematical modeling of slip weakening in geological systems, *J. Geophys. Res.*, *112*, B04301, doi:10.1029/2005JB004056.

1. Introduction

[2] Deformation of the Earth's crust from tectonic forces involves both diffuse elastic and plastic strains, rigid body translations and rotations, and localized deformations concentrated along narrow fault zones [*Anderson*, 1951; *Sibson*, 1986]. Movement along fault zones may occur either slowly by creep and/or differential slippage as well as by sudden rupture [*Bolt*, 1970; *Scholz*, 1990]. Earthquake ground motion induced by tectonic forces is interpreted to be caused by dynamic slip instability associated with rupture propagation along fault zones causing a sudden drop in shear stress [*Rice*, 1980]. The magnitude of the stress drop and the amount of slip required to realize this stress drop is quantified by the shear fracture energy and is commonly correlated with the size of an earthquake [*Rudnicki*, 1980; *Wong*, 1982; *Sibson*, 1986, 1989].

[3] Slip weakening is the process used to describe the strength degradation within the fault zone during the initial stage of slip instability. The concept was motivated by the cohesive zone models for tensile fracture developed by *Barenblatt* [1962], *Dugdale* [1960], and *Bilby et al.* [1963] and extended to the shear fracture problem by *Ida* [1972] and *Palmer and Rice* [1973]. As the Earth's crust is deformed the stress increases until it reaches a peak resistance. For intact or relatively undamaged rocks this peak resistance may consist of frictional and cohesive components along potential faults, whereas for previously faulted rocks the peak resistance may be predominantly frictional in nature, although the coefficient of friction may have increased as a result of aging of the contact. Once the peak resistance is reached intact rocks may fail by development of a new fault zone, whereas previously faulted rocks may deform by reactivation of an old fault zone or the creation of a new one depending on the current loading direction. The shear strength then decays to a lower level on those segments of the fault that slipped. This "residual" strength is commonly interpreted to be purely frictional in nature with the coefficient of friction at the residual state being generally lower than the peak value for previously faulted rocks.

[4] To better understand the process of slip weakening in earthquake fault zones, specimens of rocks have been tested in the laboratory and values of the shear fracture energy have been inferred from measurements [*Rummel et al.*, 1978; *Rice*, 1980; *Okubo and Dieterich*, 1984; *Wong*, 1982, 1986]. However, the analysis of such test data is not trivial because the stress paths are different for each type of test. For example, in the biaxial tests performed by *Okubo and Dieterich* [1984] the normal stress on the fault zone was held constant, whereas in the triaxial test results analyzed by *Wong* [1982] and *Rice* [1980] the normal stress was steadily decreasing during the slip weakening. Furthermore, the coefficient of friction may be changing during the slip-weakening process [*Dieterich*, 1979; *Ruina*, 1983], although this latter factor may have second-order effects compared to a variable normal stress which is first order. Nevertheless, from a static equilibrium configuration to the

[1]Department of Civil and Environmental Engineering, Stanford University, Stanford, California, USA.

Copyright 2007 by the American Geophysical Union.
0148-0227/07/2005JB004056$09.00

initial activation of a fault the coefficient of friction increases rapidly from zero to a nearly steady state value, and so within this very narrow time interval the effect of a variable coefficient of friction also could be first order.

[5] Construction of a slip-weakening model from compression test data on initially intact rock specimens requires transformation of postfailure data to infer the shear stress versus shear slip responses [*Wong*, 1982, 1986]. A common slip-weakening law describing the degradation of shear stress on fault zones is provided by a linear function of slip with the total shear stress dropping linearly from a peak value τ° to a residual value τ^* over a cumulative slip ζ^* [*Ida*, 1972]. During the slip nucleation process the frictional resistance picks up but its exact variation remains unknown until after the segment has slipped enough for the fault to be well defined, i.e., when the slip has reached the critical value ζ^*. Thus, whereas the slope of the straight line can be explicitly calculated from test results after the fact, it cannot be supplied as a given parameter in the analysis of a general boundary value problem because it is actually a state variable whose value depends on the final frictional resistance at residual state.

[6] This paper formulates the linear slip-weakening law implicitly by expressing the unknown frictional resistance at residual state in terms of its current value, plus some higher-order contributions arising from a Taylor series expansion. The truncated Taylor series relies on the slope of the stress path on the normal stress–shear stress (σ, τ) plane, $d\sigma/d\tau$, which is constant in conventional triaxial compression tests but could vary in a complicated way for a general three-dimensional (3-D) loading condition. For the latter case we propose an alternative simplified slip-weakening law that captures the straight line variation only in an approximate way but does not utilize the slope $d\sigma/d\tau$. The formulation has the advantage in that the linear slip-weakening law can be captured either exactly or approximately without explicitly prescribing the slope of the line.

[7] Experimental observations also suggest that the coefficient of friction for fault zones is a function of the slip speed and a state variable reflecting the maturity of contact [*Dieterich*, 1979; *Ruina*, 1983]. Therefore the frictional resistance at the residual state must also reflect this aspect in principle. Unfortunately, incorporating velocity- and state-dependent friction is not suitable for manual calculations because they are so involved mathematically. In the first place, the time integration can only be done numerically in most cases because of the coupling between slip velocity and the state variable. In the second place, the linearization that must be done to solve the inverse problem (i.e., given the load, find the displacement) with Newton iteration must reflect the coupling between these two variables. Therefore, in this paper we resort to nonlinear finite element calculations for the solution of general boundary value problems involving faulting.

[8] The finite element framework we propose in this paper relies on a technique in which a "slip tensor" is embedded into a standard finite element in order to enrich the interpolation capability of this element to resolve the displacement jump, or "strong discontinuity," occurring across it [*Borja*, 2000, 2002; *Borja and Regueiro*, 2001; *Regueiro and Borja*, 2001]. The slip tensor has two attributes: a direction defining the normal to the slip plane and another direction defining the slip. By embedding this slip tensor into the most critically stressed finite element we effectively capture fault nucleation, and by propagating this slip tensor throughout the finite element mesh we effectively capture fault growth. An advantage of the proposed approach is that we do not need to specify the most critically stressed finite element at which the fault would nucleate, nor the orientation of the fault zone: The finite element solution is expected to identify all of these aspects. Furthermore, the finite element solution is also expected to track the direction of propagation of a fault.

[9] We illustrate the finite element technique with a simple numerical example involving slip weakening combined with velocity- and state-dependent friction. The problem is analyzed quasi-statically even though rupture propagation is inherently a dynamic process. Dynamic rupture propagation, commonly encountered in earthquake fault modeling, involves fast sliding velocities and slips that are much larger than those commonly encountered in laboratory experiments. These large slips and slip rates could activate additional weakening mechanisms such as flash heating, for example, resulting in a much lower frictional resistance during dynamic sliding [*Lapusta*, 2005]. In such a case, the Dieterich-Ruina rate and friction law may have to be modified to permit much stronger weakening at high slip velocities and/or large slips, see also *Rice* [2006]. This paper focuses only on slow slip velocities and laboratory-derived state and friction laws.

2. Inelastic Continuum Modeling of Rock Mechanical Behavior

[10] The mechanical behavior of most rock types of interest to the earth scientist varies considerably with temperature, confining pressure, and strain rate. In order to limit the scope of this paper, we shall restrict the discussion to rock materials tested in the laboratory at constant temperature and under a range of confining pressures that is currently supported by available testing equipment (e.g., up to around 1000 MPa) [*Paterson*, 1990]. The mechanical behavior of these materials is typically represented by a stress-strain curve that is initially linear and has a steep slope. This stage of deformation is the elastic region because when the stress is removed the original dimension of the material is recovered completely. Some rocks may suddenly fracture, or fail in brittle mode, while still deforming in the elastic regime. The value of the stress at this point is known as the brittle strength [*Jaeger and Cook*, 1969; *Evans et al.*, 1990]. If fracture creates a shear failure plane, then the ruptured material will subsequently slip along this plane. We denote the complete Cauchy stress tensor at the point of fracture by the symbol σ°_{ij}.

[11] If the rock is not brittle, then the slope of the stress-strain curve flattens out at some point of deformation. This stage of deformation is commonly called the inelastic (or plastic) regime because when the load is removed a certain portion of deformation remains. The stress-strain curve may continue to exhibit a positive slope until eventually it reaches a certain peak stress. Typically the peak stress is accompanied by the appearance of a thin zone of shear strain localization in the sample commonly called a shear band, although this terminology has been superseded as of

late by a more general term "deformation band" to reflect the fact that other modes of deformation, such as dilation and compaction, may also be present in addition to shearing within the localized zone. We also denote the complete Cauchy stress tensor at the point of initial appearance of a deformation band by the same symbol σ°_{ij}. Hence σ°_{ij} generally represents the transition stress between an intact state to a state characterized by strain localization.

[12] For a general three-dimensional loading condition the elastic region is assumed to be bounded by a so-called yield surface defined by

$$F(\sigma_{ij}, \kappa) = 0, \tag{1}$$

where σ_{ij} is the symmetric Cauchy stress tensor and κ is a plastic variable describing the extent of the elastic region. Since plastic yielding reflects a material's constitutive behavior, the yield surface should not depend on the reference frame (i.e, it is frame-invariant). Hence, if the material behaves isotropically the yield surface may be expressed alternatively in terms of the principal stresses σ_1, σ_2, and σ_3 in the form

$$F(\sigma_1, \sigma_2, \sigma_3, \kappa) = F(\sigma_2, \sigma_1, \sigma_3, \kappa) = \ldots = 0, \tag{2}$$

where it is implied that the value of the function is the same irrespective of how one labels the principal stresses. In this case, we say that the yield function F is isotropic with respect to the stresses. It is also possible to use a yield surface with some anisotropy attached to it that is induced either by a previous loading history when a material is subjected to reverse or cyclic loading (stress-induced anisotropy), or by a homogenization of a representative volume element (RVE) of a rock mass transgressed, for example, by inherited planar defects [*Leroy and Sassi*, 2000; *Guiton et al.*, 2003]. The latter may be important for modeling rock deformations on a larger scale (say, in the order of kilometers).

[13] For the case of an isotropic yield function we can represent the yield surface conveniently in three-dimensional principal stress space. For example, Figure 1a shows the Mohr-Coulomb yield surface, a plasticity model commonly used to describe the inelastic behavior of geomaterials. The yield surface is centered about the hydrostatic axis defined by the line $\sigma_1 = \sigma_2 = \sigma_3$. On a deviatoric plane defined by the equation $\sigma_1 + \sigma_2 + \sigma_3 =$ constant, which runs perpendicular to the hydrostatic axis, the intersection of the yield surface is a closed, convex region, see, for example, Figure 1b for the cross section of the Mohr-Coulomb yield surface. On the deviatoric plane the yield surface exhibits some form of symmetry in that it intersects all three positive principal stress axes at the same distance from the center, representing the yield stress in triaxial extension. Similarly, it also intersects the negative stress axes at the same distance representing the yield stress in triaxial compression. For geomaterials such as rocks, the yield stress in compression is typically greater than the yield stress in extension. Figure 1b shows that for the Mohr-Coulomb model the ratio between the yield stress in compression to the yield stress in extension increases with the continuum friction angle ϕ of the material. Smooth approximations to the Mohr-Coulomb yield surface, such as the one proposed by *Matsuoka and Nakai* [1974] and shown in Figure 1c, may also be used. For high-porosity rocks yield surfaces are often enriched with a compression cap to better describe plastic yielding in compression as well as the initiation of so-called compaction bands [*Borja and Aydin*, 2004; *Borja*, 2004; *Aydin et al.*, 2006].

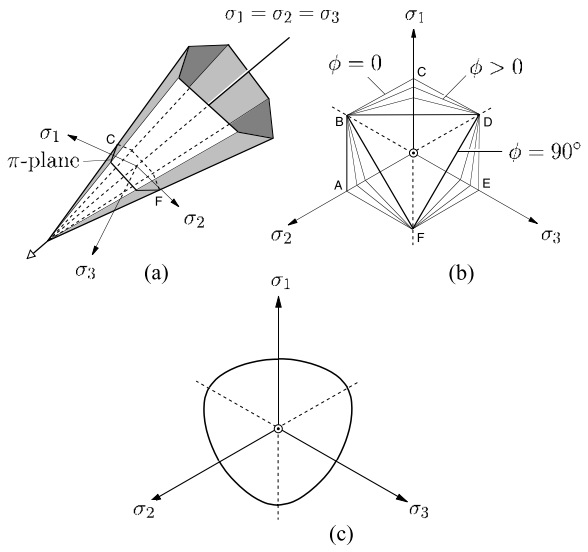

Figure 1. (a) Representation of Mohr-Coulomb (MC) yield surface in principal stress space; (b) cross sections on deviatoric plane of MC yield surfaces for different friction angles; (c) a smooth approximation of the MC yield surface.

[14] The onset of a shear band in an intact rock signifies the end of a homogeneous deformation response. Viewed as a material instability, shear bands had been investigated in the past based on the works of *Hadamard* [1903], *Hill* [1958], *Thomas* [1961], and *Mandel* [1966] within the context of acceleration waves in solids. For geological materials, *Rudnicki and Rice* [1975] presented a condition for the onset of a shear band, embodied by the classical equation

$$\det(\mathbf{A}) = 0\,, \qquad A_{ik} = n_j c^{\mathrm{ep}}_{ijkl} n_l, \tag{3}$$

where c^{ep}_{ijkl} is the rank four elastoplastic constitutive operator and n_j and n_l define components of the unit normal vector $\mathbf{n}$ to the band. The rank two tensor $\mathbf{A}$ is known in the literature as the acoustic tensor, and the determinant of this tensor as the localization function.

[15] The localization function is assumed to be initially positive for any orientation $\mathbf{n}$. As the material deforms and its stiffness degrades, the value of the localization function decreases. At a certain point in the loading history where the localization function crosses the value zero, bifurcation into a shear band occurs, and the orientation of the emerging shear band is described by the vector $\mathbf{n}$. Because the material is yielding at this particular point of deformation, the stress point is instantaneously on the yield surface, and so we have

$$F\left(\sigma^{\circ}_{ij}, \kappa^{\circ}\right) = 0, \tag{4}$$

where κ° defines the size of the elastic region at the point of bifurcation and σ_{ij}° is the bifurcation stress.

3. Formulation of Slip-Weakening Model: Linear and Simplified Laws

[16] We assume that the slip surface is defined by a unit normal vector **n** (with components n_i). If σ_{ij} is the continuum stress tensor, then the resolved normal and tangential shear stresses (σ and τ, respectively) on the slip surface may be calculated as

$$\sigma = \sigma_{ij} n_i n_j, \qquad \tau = \sqrt{t_i t_i}, \qquad t_i = \sigma_{ij} n_j - \sigma n_i . \tag{5}$$

Here we have used the strength of materials convention for the Cauchy stress where a normal stress component is positive under tension. For later use we define the stress path on the σ-τ plane by the slope

$$\frac{\delta\sigma}{\delta\tau} = \frac{n_i n_j \delta\sigma_{ij}}{\xi_{kl}\delta\sigma_{kl}}, \qquad \delta\tau \neq 0, \tag{6}$$

where

$$\xi_{kl} = \frac{1}{2}(\nu_k n_l + \nu_l n_k), \qquad \nu_k = t_k/\tau. \tag{7}$$

We identify ν_k as a component of a (normalized) unit traction vector tangent to the slip surface. In the above expression for the stress path we assume that deformations are sufficiently small so that the orientation vector **n** for the slip surface may be considered essentially constant during the slip weakening. Furthermore, the case $\delta\tau = 0$ is simply a "horizontal" stress path.

[17] Next, we define the slip velocity vector as

$$[\![\mathbf{v}]\!] = \dot{\zeta}\mathbf{m}, \tag{8}$$

where **m** is a unit vector in the direction of slip and $\dot{\zeta}$ is the magnitude of the slip rate. Typically, **m** is tangent to the slip surface although some minor variations may be observed on a smaller scale depending on the interaction of comminuted particles with the slip surface. The cumulative slip is defined by the integral

$$\zeta = \int_t \dot{\zeta}\, \mathrm{d}t, \tag{9}$$

where the integration is taken over the slip path.

[18] To make the above equations more physically meaningful, we consider an initially intact rock sample subjected to triaxial loading with σ_1, σ_2, and σ_3 representing the major, intermediate, and minor compressive principal stresses, respectively, as shown in Figure 2a. All of these principal stresses act on the faces of the specimen, with σ_2 representing the out-of-plane normal stress. A slip surface forms on the plane defined by σ_1 and σ_3 and inclined at an angle ϑ relative to σ_1. The normal and shear stresses on the slip plane are given by

$$\sigma = \sigma_1 \sin^2\vartheta + \sigma_3 \cos^2\vartheta, \quad \tau = \frac{1}{2}(\sigma_3 - \sigma_1)\sin 2\vartheta. \tag{10}$$

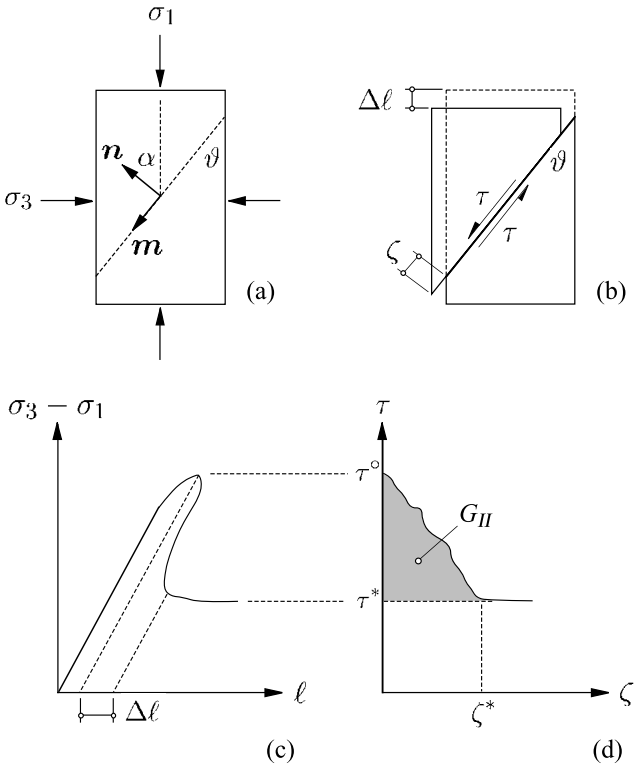

Figure 2. Shear strain localization of an initially intact rock sample: (a) condition at localization; (b) postlocalization defining relative slip assuming rigid shearing bodies; (c) global stress compression response of sample; (d) inferred slip-weakening response [after *Wawersik and Brace*, 1971].

During the slip weakening, the compressive stress σ_1 is reduced while σ_3 remains fixed; hence the stress path is given by the constant slope

$$\frac{\delta\sigma}{\delta\tau} = -\frac{2\sin^2\vartheta}{\sin 2\vartheta} = -\tan\vartheta. \tag{11}$$

On the other hand, Figure 2b shows that if the sliding blocks are relatively rigid the slip ζ can be related to the incremental axial shortening $\Delta\ell$ according to the approximate relation

$$\zeta = \Delta\ell/\cos\vartheta. \tag{12}$$

As the slip ζ builds up the resolved shear stress τ decreases until it reaches a steady state value called the residual shear stress τ^* when the slip has reached the critical value ζ^*. We are interested in developing a slip-weakening constitutive law describing the reduction of shear stress τ with slip over the region $\zeta \in \lfloor 0, \zeta^* \rfloor$.

[19] Figures 2c and 2d demonstrate how to transform the stress-displacement test data to infer the postlocalization τ-ζ response [see *Wong*, 1982, 1986]. The overall specimen response depicted in Figure 2c represents a class I behavior in which the maximum principal stress difference decreases so dramatically at postlocalization, assumed in Figure 2c to occur at the peak point, that the stress displacement curve

turns over so far as to follow a positive slope [*Wawersik and Fairhusrt*, 1970; *Wawersik and Brace*, 1971]. This is in contrast to a more regular class II stress drop with a negative slope. Assuming that the elastic Young's modulus remains constant during the test, then $\Delta\ell$ at postlocalization is calculated as shown in Figure 2c, and the shear strength-slip displacement curve may be constructed as shown in Figure 2d.

[20] The shear stress-slip curve shown in Figure 2d has a peak value of τ° at the beginning of the slip weakening. The shear strength mobilized on the slip plane then decreases until it stabilizes to a residual value τ^* when the slip has reached a value approximately equal to $\zeta^* \approx 0.5$ mm for most rocks [*Wong*, 1982; J. R. Rice, personal communication, 2005]. Thereafter, the shear stress remains essentially constant at this residual value. By comparison, *Ohnaka et al.* [1997] presented shear stress–slip displacement curve for faulting in an initially intact rock with the shear stress first increasing to a peak value at "apparent" slip displacement equal to D_a, then dropping to the residual value at ζ^*. The Ohnaka et al. curve was obtained by subtracting the linear elastic response but not the bulk plastic response prior to localization, and so in principle their peak stress takes the same meaning as the stress τ° used in the present paper. Although the slip-weakening curve may exhibit some slight irregularities, a linear slip-weakening law is usually assumed and takes the form [*Ida*, 1972; *Campillo and Ionescu*, 1997; *Uenishi and Rice*, 2003; *Rice and Cocco*, 2007]

$$\tau_f = \tau^\circ - (\tau^\circ - \tau^*)\frac{\zeta}{\zeta^*}, \qquad \zeta \in [0, \zeta^*]. \tag{13}$$

This law satisfies the essential conditions $\tau_f = \tau^\circ$ at $\zeta = 0$ and $\tau_f = \tau^*$ at $\zeta = \zeta^*$. The given parameters are τ°, which we determine from (5) at the transition stress σ°_{ij}, and the critical slip ζ^*.

[21] The problem with equation (13) is that neither the residual shear stress τ^* nor the slope $-(\tau^\circ - \tau^*)/\zeta^*$ is known since the constitutive properties of the slip surface as well as the normal stress acting on this surface may be changing during the slip weakening process. Hence it is not possible to compute the total stress drop $\Delta\tau = \tau^\circ - \tau^*$ until after the residual shear stress has already been calculated. On the other hand, the residual shear stress τ^* in rock faults arises only from pure friction, so if we assume a coefficient of friction on the slip surface μ then the frictional shear resistance is $f = -\mu\sigma$, and hence $\tau^* = f^* = -\mu^*\sigma^*$. The current value of f is always known during the slip weakening process, so our objective is then to express f^* in terms of the known value of the frictional shear stress f. The key point here is to treat the slope $-\Delta\tau/\zeta^*$ implicitly, rather than explicitly, as demonstrated below.

[22] Expanding f^* about f using the Taylor series expansion gives

$$\begin{aligned}\tau^* = f^* &= f + \frac{\partial f}{\partial \zeta}(\zeta^* - \zeta) + \frac{1}{2!}\frac{\partial^2 f}{\partial \zeta^2}(\zeta^* - \zeta)^2 + \dots \\ &\approx f + \frac{\partial f}{\partial \zeta}(\zeta^* - \zeta),\end{aligned} \tag{14}$$

where we have ignored the terms in the Taylor series involving the second and higher derivatives. The coefficient

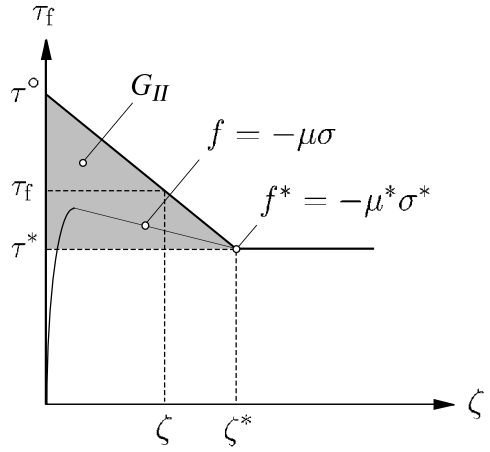

Figure 3. Graphical representation of linear slip weakening. As shear stress weakens linearly to residual value, frictional resistance picks up while cohesion decays to zero. The shear fracture energy is represented by the shaded area of triangle.

of friction μ may also depend on the slip rate, as elaborated further in section 4, but its effect is usually second order in comparison to that of a variable σ, so ignoring the variation of μ we simply write

$$\frac{\partial f}{\partial \zeta} = -\mu\frac{\partial \sigma}{\partial \zeta} = -\mu\frac{d\sigma}{d\tau}\frac{\partial \tau}{\partial \zeta}, \tag{15}$$

where $d\sigma/d\tau$ is the slope of the stress path given by equation (6) for a general 3-D continuum loading. For continued slip weakening, $\tau = \tau_f$; so imposing the linear slip weakening law, we get

$$\frac{\partial f}{\partial \zeta} = -\mu\frac{d\sigma}{d\tau}\frac{\partial \tau_f}{\partial \zeta} = -\mu\frac{d\sigma}{d\tau}\left(\frac{\tau_f - \tau^\circ}{\zeta}\right), \quad \zeta \neq 0, \tag{16}$$

where the quantity inside the parentheses represents the constant slope $\partial\tau_f/\partial\zeta$ implied by the linear slip-weakening constitutive law (see Figure 3). Note that this slope is also equal to $(\tau^* - \tau^\circ)/\zeta^*$, as shown in Figure 3, but as noted before, τ^* is yet to be calculated so this latter expression cannot be used.

[23] Substituting this result into (14) yields

$$\tau^* = f - \mu\frac{d\sigma}{d\tau}\left(\frac{\tau_f - \tau^\circ}{\zeta}\right)(\zeta^* - \zeta), \qquad \zeta \neq 0. \tag{17}$$

The above expression depends only on the current state variables ζ, f, τ_f, and the slope $d\sigma/d\tau$. Inserting this expression into the linear slip-weakening constitutive law (13) then gives

$$\tau_f = \chi^{-1}\tau^\circ(1 - \eta)\left(1 + \mu\frac{d\sigma}{d\tau}\right) + \chi^{-1} f\eta, \tag{18}$$

where

$$\chi = 1 + \mu(1 - \eta)\frac{d\sigma}{d\tau}, \qquad \eta = \zeta/\zeta^*. \tag{19}$$

Like equation (13), equation (18) also satisfies the conditions $\tau_f = \tau^\circ$ at $\eta = 0$, and $\tau_f = f^*$ at $\eta = 1$.

[24] To elucidate the above slip-weakening law, we consider a triaxial compression test reported by *Wong* [1986] on sample G3 of San Marcos gabbro. The test was conducted by varying the major compressive stress σ_1 while holding σ_2 and σ_3 fixed. Assuming the principal stress directions remained fixed during the test, the instantaneous stress path is given by the slope $d\sigma/d\tau = -\tan\vartheta$, where the physical significance of ϑ is shown in Figure 2. *Wong* [1986] reported a confining stress $\sigma_3 = -250$ MPa, which was held constant during the test. At peak, the stresses were $\tau^\circ = 433$ MPa and $\sigma^\circ = -500$ MPa; at residual, they were $\tau^* = 326$ MPa and $\sigma^* = -439$ MPa. We back figured the coefficient of friction at residual state to be $\mu^* = -\tau^*/\sigma^* = 0.743$, which we assumed constant in the present analysis. The total drops in the normal and shear stresses were $\Delta\sigma = \sigma^* - \sigma^\circ = 61$ MPa and $\Delta\tau = \tau^* - \tau^\circ = -107$ MPa, respectively, and so from (11) we calculated $\vartheta = \tan^{-1}(-\Delta\sigma/\Delta\tau) = 30^\circ$. This agrees with a reported angle of $\alpha = 90^\circ - \vartheta = 60^\circ$ in Table 1 of *Wong* [1986]; see Figure 2a for the physical significance of the angle α.

[25] Now we use equation (18) to predict the slip-weakening response. First, we substitute $d\sigma/d\tau = -\tan\vartheta$ into (18) and (19). Since the material is slipping continually, $\tau_f = \tau$. Inserting (10) into the expressions for $f = -\mu\sigma$ and τ, and ignoring the variation of μ, we obtain the expected variation of σ_1 during this test as follows:

$$\sigma_1 = \frac{\sigma_3[\mu\eta\cos^2\vartheta + (\chi\sin 2\vartheta)/2] - \tau^\circ(1-\eta)(1-\mu\tan\vartheta)}{(\chi\sin 2\vartheta)/2 - \mu\eta\sin^2\vartheta} = \sigma_3\left[1 + \frac{2\mu}{(1-\mu\tan\vartheta)\sin 2\vartheta}\eta\right] - \frac{2\tau^\circ}{\sin 2\vartheta}(1-\eta), \tag{20}$$

where $\chi = 1 - \mu(1-\eta)\tan\vartheta$. The second line of equation (20) describes a linear drop of σ_1 with $\eta = \zeta/\zeta^*$. That we recover a linear drop exactly is hardly surprising since τ is postulated to drop linearly with η, so σ will also drop linearly since we assumed a constant coefficient of friction μ and $d\sigma/d\tau$ is constant. This implies that f will also vary linearly with η, and so only the first derivative of f in the Taylor series is needed to determine the exact residual value f^*.

[26] Figure 4 shows a plot of equation (20) for sample G3 of San Marcos gabbro. For this simulation, 10- and 100-increment solutions were performed and the predicted variation of σ_1 is perfectly linear for either case. We emphasize that the calculations shown in Figure 4 did not make use of the residual shear stress τ^* even though this information was provided by *Wong* [1986]. In fact, substituting (20) into the expression for τ in (10) gives the following linear slip weakening constitutive law for the triaxial compression test performed by Wong:

$$\tau_f = \tau^\circ(1-\eta) - \frac{\mu\sigma_3}{1-\mu\tan\vartheta}\eta. \tag{21}$$

Again, equation (21) meets both end conditions with $\tau_f = \tau^\circ$ at $\eta = 0$, and $\tau_f = -\mu\sigma^*$ at $\eta = 1$ after noting that $\sigma^* = \sigma_3/(1-\mu\tan\vartheta)$ for σ_1 obeying (20). For completeness, we show in Figure 5 a 3-D plot in the (ζ, f, τ_f) space of equation (20) for this test.

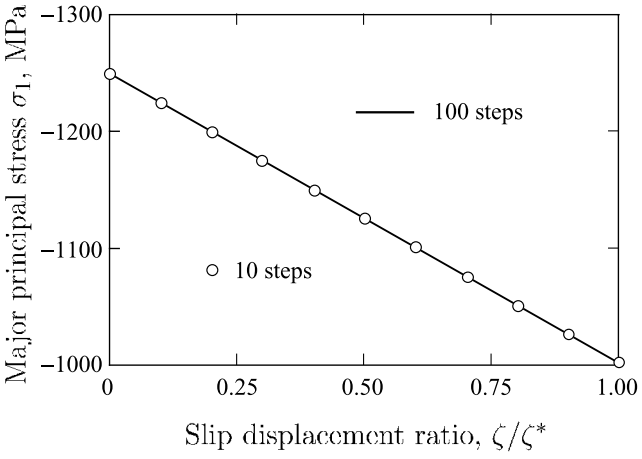

Figure 4. Linear drop of major principal stress during triaxial testing of San Marcos gabbro (sample G3) manifested by 10 and 100 load step solutions. The two solutions are identical to machine precision.

[27] For a general boundary value problem equation (20) requires the evaluation of the slope $d\sigma/d\tau$ of the stress path, which could make the calculations unwieldy. For the triaxial test example described above this slope was constant, but in a general 3-D continuum problem this slope is expected to vary in an unpredictable way. Furthermore, if the motion of the continuum is large so as to alter the orientation of the slip surface, then even the unit vector **n** is expected to vary, thus making the evaluation of the slope $d\sigma/d\tau$ very cumbersome. To alleviate this difficulty, we drop the first derivative in the Taylor series altogether and simply write $\tau^* \approx f$. This leads to a simplified slip-weakening constitutive law of the form

$$\tau_f = \tau^\circ - (\tau^\circ - f)\frac{\zeta}{\zeta^*}. \tag{22}$$

Equation (22) is simpler than (20); however, it does not recover completely the linear slip-weakening law since the Taylor series expansion was short by one term. On the other hand, equation (22) still satisfies the two essential end conditions at τ° and $\tau^* = f^*$. Hence, under normal conditions we expect the deviation of (22) from a linear constitutive law to be "mild."

[28] Repeating the analysis of the previous example, we set $\tau_f = \tau$ and $f = -\mu\sigma$, and again substitute equation (10) into the simplified law (20) to obtain the expected drop of σ_1 with slip for sample G3 of San Marcos gabbro as follows:

$$\sigma_1 = \frac{\sigma_3[\mu\eta\cos^2\vartheta + (\sin 2\vartheta)/2] - \tau^\circ(1-\eta)}{(\sin 2\vartheta)/2 - \mu\eta\sin^2\vartheta}, \quad \eta = \zeta/\zeta^*. \tag{23}$$

Figure 6 compares the simplified slip-weakening relation (20) with the linear law and suggests that σ_1 drops more slowly in the beginning but catches up toward the end as the slip reaches the critical value ζ^*. The shear fracture energy, represented in Figure 2d by the shaded area and denoted by the symbol G_{II}, is thus overpredicted by about 15% relative to that computed with the linear law. Figure 7 shows a three-

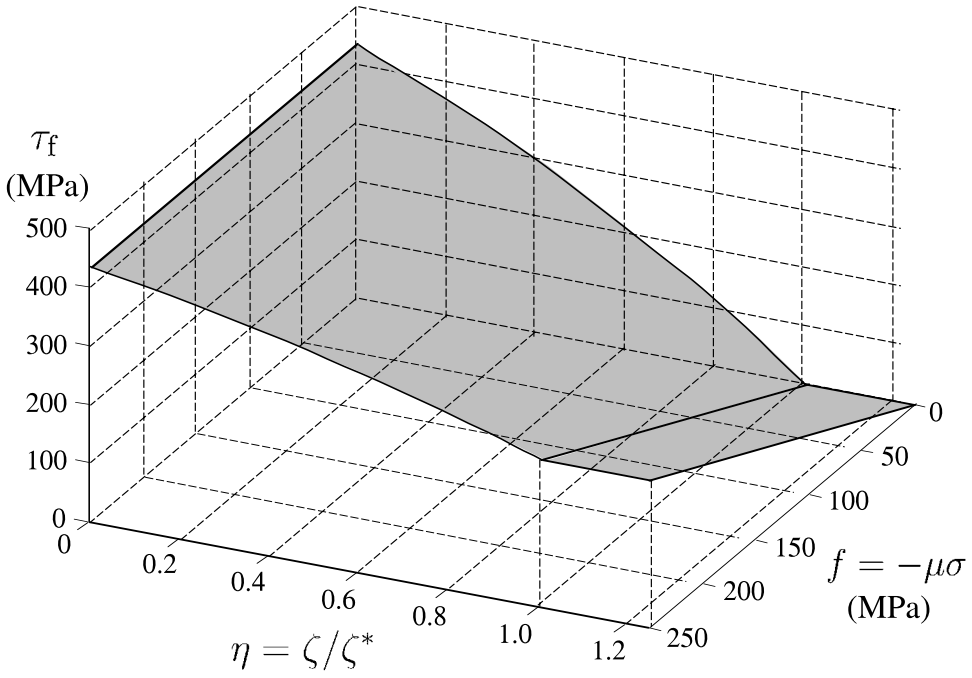

Figure 5. Exact linear slip-weakening function for triaxial test simulation of San Marcos gabbro (sample G3) with constant coefficient of friction. Note that $\eta \geq 1$ denotes residual condition.

dimensional plot of (20) in the (ζ, f, τ_f) space and defines a warped surface. It suggests that if f increases (alternatively, decreases) during the slip weakening, then the projection of the state path on the (τ_f, ζ) plane is slightly concave upward (alternatively, downward). The deviation from the linear law depends on how drastically the normal stress σ varies during the slip weakening. Interestingly, *Ida* [1972] also considered similar nonlinear slip-weakening laws exhibiting upward and downward concavities relative to the linear law.

4. Variable Friction Model

[29] Figure 8 represents pictorially the slip-weakening process on the deviatoric plane. We assume here that the slip surface is triggered by a shear band-type bifurcation, so the transition stress σ°_{ij} lies on the yield surface $F(\sigma^\circ_{ij}, \kappa^\circ) = 0$. Figure 8 shows two cross sections of a conical three-invariant yield surface, one cutting through a plane $\sigma_1 + \sigma_2 + \sigma_3 = \sigma^\circ_{ii} = C < 0$ (light curve) at the point of bifurcation, and a second cutting through the π plane defined by the equation $\sigma_1 + \sigma_2 + \sigma_3 = 0$ (heavy curve). The stress paths are all projected to the π plane. We assume that the initial shear resistance acting on the emerging shear band is of the Mohr-Coulomb type,

$$\tau_f = c - \mu\sigma, \tag{24}$$

where c is cohesion. At the bifurcation stress the shear stress on the band is $\tau^\circ = c^\circ - \mu^\circ\sigma^\circ$, while at the residual state a purely frictional resistance gives $\tau^* = -\mu^*\sigma^*$. During the

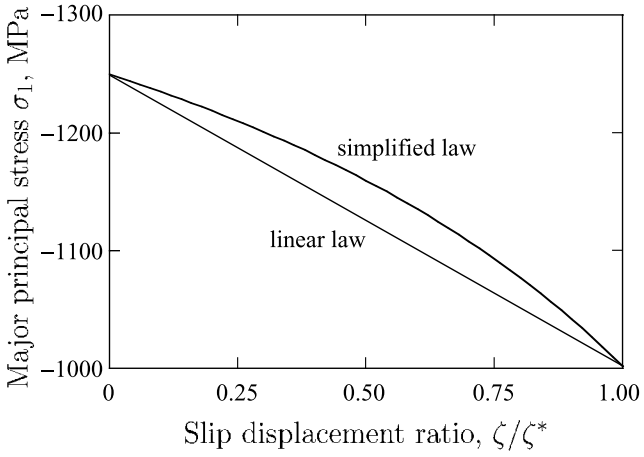

Figure 6. Predicted drop of major principal stress during triaxial testing of San Marcos gabbro (sample G3). The simplified law is concave downward relative to the linear law since f decreases during slip weakening for this test.

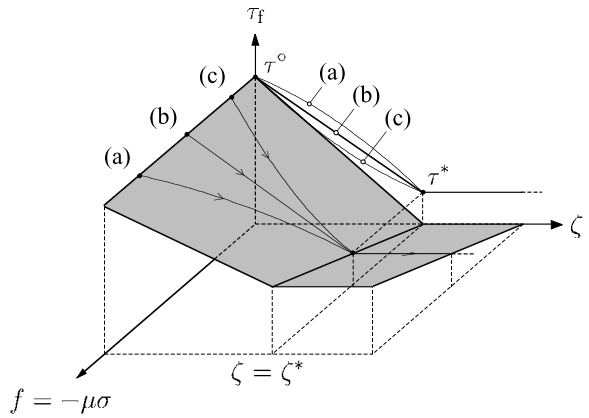

Figure 7. Graphical representation of simplified slip-weakening function: curve a, f decreasing; curve b, f constant; curve c, f increasing.

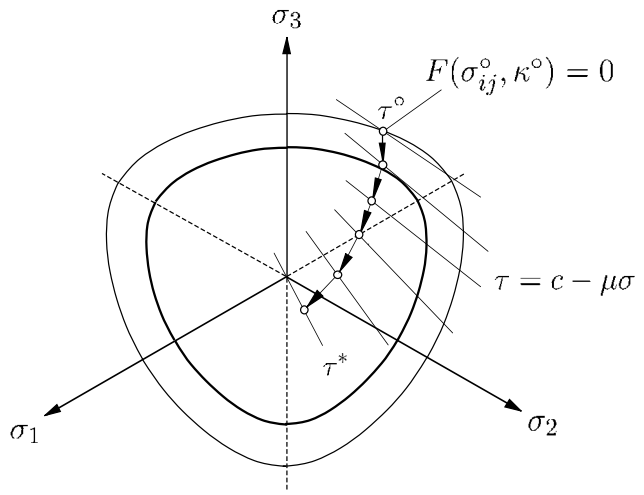

Figure 8. Pictorial representation of slip weakening on the π plane. Fan of straight lines represents the Mohr-Coulomb failure criterion for a planar fault; at residual state the cohesion decays to zero; hence the failure criterion passes through the origin.

slip weakening the cohesive resistance dies out to zero while the frictional resistance picks up. This feature is also manifested in Figure 3 which further shows that this frictional resistance generally could vary during the slip weakening process in an unpredictable way. This interplay between the two types of resistance is represented in Figure 8 by the changing slopes of lines representing equation (24). In this section we provide an in-depth look into this interplay between the two types of resistance in a more quantitative way.

[30] Early experimental observations suggest that the coefficient of friction μ mobilized on the surface of discontinuity between two contacting bodies subjected to a slowly increasing load is a function of the slip speed $\dot{\zeta}$ and a state variable θ reflecting the maturity of the contact. Under conditions of fixed temperature an empirical law of the following form has been proposed by *Dieterich* [1979], *Ruina* [1983], and *Dieterich and Linker* [1992],

$$\mu = \mu_0 + A \ln\left(\frac{\dot{\zeta}}{a}\right) + B \ln\left(\frac{\theta}{b}\right), \tag{25}$$

where μ_0, A, and B are experimentally determined constants, and a and b are normalizing constants. For rocks, typical values of A and B range from 0.005 to 0.015.

[31] The role of θ is to reflect contact aging, or lifetime. An empirical evolution equation for θ first proposed by *Ruina* [1983] takes the form

$$\frac{d\theta}{dt} = 1 - \frac{\theta\dot{\zeta}}{D_c}, \tag{26}$$

where D_c may be interpreted as the characteristic slip required to replace a contact population representative of a previous sliding condition with a contact population created under a new sliding condition; it may be approximated as the mean contact diameter on the order of 10 μm [*Dieterich and Kilgore*, 1996]. This law allows for friction hardening of the material over time and is known as the healing form of the evolution equation. If $\dot{\zeta} = 0$, then (26) indicates that θ increases by an amount equal to the elapsed time of stationary contact, reflecting contact aging. If $d\theta/dt = 0$, then the steady state value of θ is $\theta_{ss} = D_c/\dot{\zeta}$. Substituting this value in (25) gives

$$\mu_{ss}|_{\dot{\zeta}_1} = \mu_{ss}|_{\dot{\zeta}_2} + (A - B) \ln\left(\frac{\dot{\zeta}_2}{\dot{\zeta}_1}\right). \tag{27}$$

If the requirement that steady state friction decreasing with slip speed is imposed, then the relation $A < B$ must hold [*Ruina*, 1983; *Rice and Ruina*, 1983].

[32] A drawback of the logarithmic form of friction law is that this expression is singular when the slip velocity is zero. Hence it cannot be used to describe what occurs during initiation of a slip surface. Although based solely on empirical observations, this expression, however, has a theoretical basis if one considers friction sliding as a rate process [*Chester and Higgs*, 1992; *Mitchell*, 1993; *Lapusta et al.*, 2000; *Rice and Cocco*, 2007]. Writing $\mu = -\tau/\sigma = -\tau_c/\sigma_c$, where τ and σ are macroscopic shear and normal stresses, and τ_c and σ_c are the corresponding contact stresses, respectively, equation (25) can be solved for slip velocity as

$$\dot{\zeta} = a \exp\left[-\frac{(E - \tau_c\Omega)}{RT}\right], \tag{28}$$

where the following substitutions have been made:

$$\frac{E}{RT} = \frac{\mu_0}{A} + \frac{B}{A} \ln\left(\frac{\theta}{b}\right), \quad \frac{\Omega}{RT} = -\frac{1}{A\sigma_c}. \tag{29}$$

If one interprets E as the activation energy, $\tau_c\Omega$ as the directional energy over a sampling volume Ω, R as the universal gas constant, and T as absolute temperature, then equation (28) is nothing else but a truncated Arrhenius equation considering only forward jumps during forward sliding.

[33] Terms representing the backward jumps during forward sliding in a rate process are usually very small except when the directional energy $\tau_c\Omega$ is close to zero. This explains why the Dieterich-Ruina law matches the observed test results quite well. However, when $\tau_c\Omega$ is close to zero the complete Arrhenius equation must be considered,

$$\begin{aligned}\dot{\zeta} &= a\left\{\exp\left[-\frac{(E - \tau_c\Omega)}{RT}\right] - \exp\left[-\frac{(E + \tau_c\Omega)}{RT}\right]\right\} \\ &= 2a \exp\left(-\frac{E}{RT}\right) \sinh\left(\frac{\tau_c\Omega}{RT}\right).\end{aligned} \tag{30}$$

Solving back for $\mu = -\tau_c/\sigma_c$ then yields the regularized constitutive law for velocity- and state-dependent friction

$$\mu = A \sinh^{-1}\left\{\frac{\dot{\zeta}}{2a} \exp\left[\frac{\mu_0}{A} + \frac{B}{A} \ln\left(\frac{\theta}{b}\right)\right]\right\}. \tag{31}$$

At $\tau_c\Omega = 0$ the forward and backward jumps are statistically equal, resulting in $\dot{\zeta} = 0$ and $\mu = 0$. This regularized form for

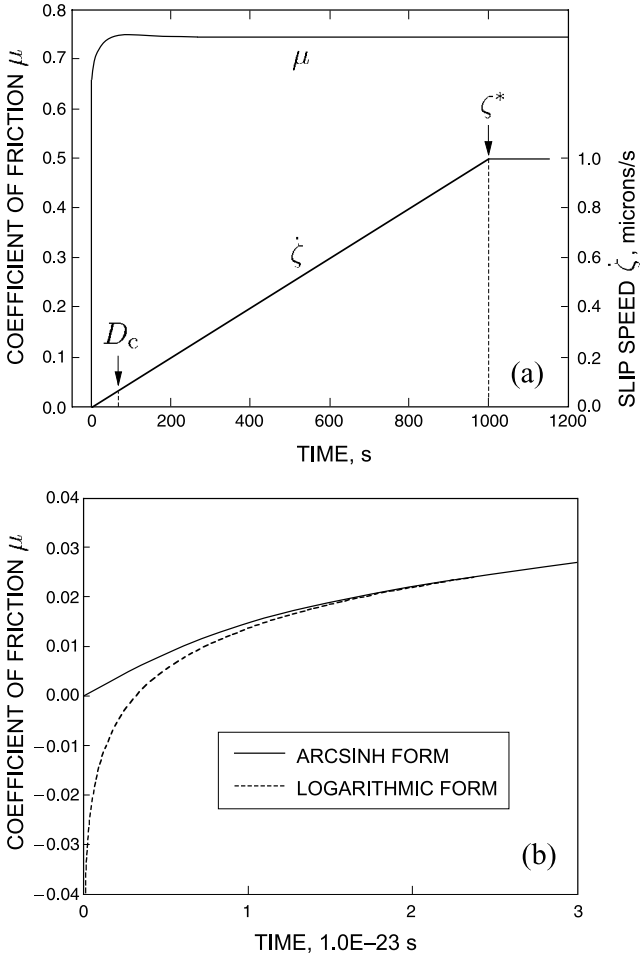

Figure 9. Variation of coefficient of friction μ: (a) variation during slip weakening and (b) comparison between arcsinh and logarithmic functions.

μ has been used by *Rice and Ben-Zion* [1996] and *Ben-Zion and Rice* [1997]. Equation (31) may be combined with the evolution law for θ given by (26) to obtain a direct constitutive law between μ and $\dot{\zeta}$, eliminating θ as an independent variable in the process. This may be done either analytically or numerically.

[34] Figure 9 compares expressions (25) and (31) for sample G3 of San Marcos gabbro analyzed earlier. To make the comparison, these two expressions were combined with Ruina's healing law (26) and solved numerically by trapezoidal integration. The material parameters used were A = 0.012, B = 0.0135, D_c = 2.25 μm, μ_0 = 0.743, a = 1 μm/s, and b = 2.25. The value of μ_0 was selected so that at a slip speed of 1 μm/s we recover the steady state coefficient of friction of 0.743 (see section 3); otherwise, the remaining parameters were taken from fits to experimental data for a granite [*Linker and Dieterich*, 1992]. Note that for the most part the two expressions for μ result in curves that lie one on top of the other except at extremely small slip displacements (near-zero velocity) where expression (25) becomes singular.

[35] As noted in equation (15), the variation in μ is second-order compared to the variation of the normal stress (except at very small slip displacements on the order $\zeta < D_c$), so the linear slip-weakening form (18) holds even for a variable coefficient of friction. Combining this with (24) yields an expression for cohesion of the form

$$c = \chi^{-1}\tau^{\circ}(1-\eta)\left(1+\mu\frac{d\sigma}{d\tau}\right) + \chi^{-1}f\eta + \mu\sigma, \qquad (32)$$

where χ is given in equation (19). On the other hand, if we use the simplified slip-weakening law (22), then we get the following evolution for c:

$$c = \tau^{\circ} - (\tau^{\circ} - f)\frac{\zeta}{\zeta^*} + \mu\sigma = (\tau^{\circ} + \mu\sigma)\left(1 - \frac{\zeta}{\zeta^*}\right). \qquad (33)$$

In either case, as the frictional resistance picks up the cohesion c inherits the "softening" character of τ_f since it is simply equal to τ_f translated by the distance $\mu\sigma$.

5. Embedding a Slip Tensor Into a Finite Element

[36] There are at least two ways of implementing the slip-weakening model in a finite element framework. First, if we know where the slip surface begins and the direction it propagates we can use standard stick-slip contact elements and construct a grid such that the slip surface is traced by the sides of the finite elements. The slip-weakening model can then be used by the contact elements in the form of a stick-slip constitutive law, allowing the nodal connections to rupture on the element sides. However, this is not a robust approach since in general we do not know where the slip surface will nucleate and what direction it will propagate. A second approach would be to allow a standard finite element to break somewhere in the middle as soon as an instability is detected in this element. This can be made possible by embedding a slip tensor into the finite element to resolve the displacement jump, also called "strong discontinuity" in the computational mechanics literature. This section focuses on the implementation of the proposed slip-weakening model using the embedded strong discontinuity approach.

[37] The underlying idea behind the finite element implementation is elucidated in Figure 10 (see *Borja* [2000, 2002] for the relevant mathematical background). Here we show a standard constant strain triangle (CST) finite element traced by a slip surface $\mathcal{S}^e$. For simplicity we only focus on 2-D plane strain problems. Figure 10a shows the element rupturing along the surface $\mathcal{S}^e$ and breaking into two parts, Ω^e_- and Ω^e_+. Let $\mathbf{u} = \mathbf{u}(\mathbf{x}^e)$ represent the displacement field inside this element. Mathematically, we have

$$\mathbf{u} = \bar{\mathbf{u}} + [\![\mathbf{u}]\!]H_{\mathcal{S}}(\mathbf{x}^e), \qquad H_{\mathcal{S}} = \begin{cases} 1 & \text{if } \mathbf{x}^e \in \Omega^e_+; \\ 0 & \text{if } \mathbf{x}^e \in \Omega^e_-. \end{cases} \qquad (34)$$

In equation (34), $H_{\mathcal{S}}$ is the Heaviside function, $\bar{\mathbf{u}}$ is the continuous part of $\mathbf{u}$, and $[\![\mathbf{u}]\!]$ is the displacement jump across $\mathcal{S}^e$ (see Figure 10b).

[38] Assuming $\mathbf{u}$ is uniform inside the element, the displacement gradient can be obtained using theory of distribution as follows [see *Stakgold*, 1998]:

$$\frac{\partial u_i}{\partial x_j} = \frac{\partial \bar{u}_i}{\partial x_j} + [\![u_i]\!]n_j\delta_{\mathcal{S}}, \qquad (35)$$

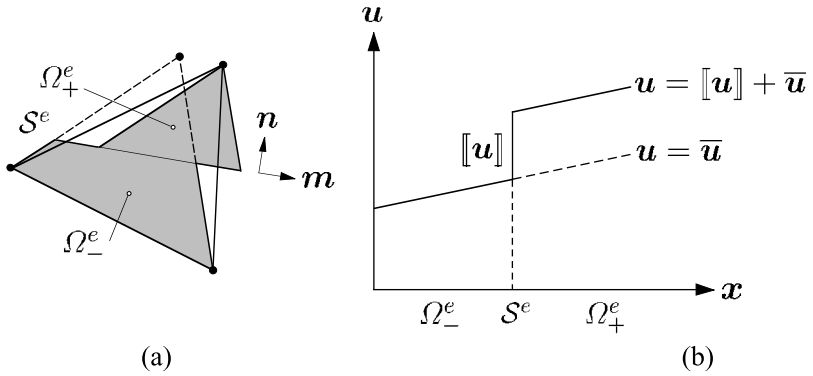

Figure 10. Enhancing a CST finite element: (a) triangle breaks into two parts and (b) displacement field with a jump across a slip plane.

where $\delta_{\mathcal{S}}$ is the Dirac delta function and n_j is the jth component of the unit normal vector **n** to the slip surface $\mathcal{S}^e$ (see Figure 10a). Similarly, we can write the velocity gradient as

$$\frac{\partial v_i}{\partial x_j} = \frac{\partial \overline{v}_i}{\partial x_j} + \dot{\zeta}\omega_{ij}\delta_{\mathcal{S}}, \tag{36}$$

where

$$\omega_{ij} = m_i n_j \tag{37}$$

is the unit slip tensor, $v_i = \dot{u}_i$, etc., and $\dot{\zeta} m_i = v_i$ is the same relation introduced in equation (8). Finally, the strain rate inside the element is given by the symmetric component of velocity gradient,

$$\dot{\varepsilon}_{ij} = \dot{\overline{\varepsilon}}_{ij} + \frac{1}{2}\dot{\zeta}\left(\omega_{ij} + \omega_{ji}\right)\delta_{\mathcal{S}}. \tag{38}$$

We note that the strain rate is singular on $\mathcal{S}^e$ because the velocity field is discontinuous across this surface. Roughly speaking then, we want to embed the slip tensor defined above into a finite element interpolation so as to enhance its capability to resolve both the coarse- and fine-scale parts of the strain field.

[39] To determine how fast the element ruptures we need to know the slip rate $\dot{\zeta}$. The slip rate in turn depends on the rate at which the external load is changing as well as on the rate of slip weakening on the rupture zone. If the fault remains active, then $\tau = \tau_{\mathrm{f}}$. The slip tensor has a dual role in this case since $\nu_i = m_i$ for 2-D problems (see (7)), so $\tau = \sigma_{ij} m_i n_j = \sigma_{ij}\omega_{ij}$. To keep the material in equilibrium, we need to satisfy the consistency condition

$$\dot{\sigma}_{ij}\omega_{ij} - \dot{\tau}_{\mathrm{f}} = 0. \tag{39}$$

The specific form of the slip-weakening constitutive law may be used to determine $\dot{\tau}_{\mathrm{f}}$. We can readily see that all of these features, along with a rate- and state-dependent coefficient of friction, are not suitable for manual calculations because the variables are intricately related in a highly nonlinear way. However, they are perfectly suitable for finite element implementation along the lines of the strong discontinuity approach. To highlight the essential aspects of the solution, we omit details of the finite element implementation and simply present a finite element simulation of the same triaxial compression test on sample G3 of San Marcos gabbro. The final example described below highlights the combined effects of slip weakening and rate- and state-dependent friction using finite elements with enhanced strain interpolation to accommodate displacement discontinuities across them.

[40] The finite element simulation is designed to replicate the test of sample G3 to the best of the available information. The properties for the slip surface are the same as for the previous example in section 4. The boundary value problem is a 2-D plane strain approximation of the triaxial test, and is conducted on a finite element mesh 0.04 m wide, 0.08 m tall and 1 m thick. The simulation is run quasi-statically, that is, inertial effects are ignored. In the horizontal direction the confining pressure of 250 MPa is applied. Then a vertical displacement 8.66 μm/s is applied. *Wong* [1986] did not specify a deformation rate. Since $D_c = 2.25$ μm to $\zeta^* = 0.5$ mm, we expect that steady state friction will be nearly fully developed by the time slip weakening has finished. Hence this rate is chosen so that for rigid sliding along a surface with $\vartheta = 30°$, the slip rate is 1 μm/s, and the steady state friction coefficient of 0.743 is recovered.

[41] Unlike the previous examples, however, the bulk sample is not rigid but is elastoplastic. Again, since material parameters are not specified, typical values for Young's modulus, 90 GPa, and Poisson's ratio, 0.15, are selected for the gabbro. Plasticity is governed by a simple Drucker-Prager model. For simplicity, an associative version of the model was used, with the cohesive strength parameter set to 8.034 MPa, the friction and dilation parameters β and b to 0.633, and the hardening modulus to -10 MPa (see *Regueiro and Borja* [2001], for example, for the physical significance of these parameters). These parameters were fit to the model so that it would fail when the first principal stress reached -1250 MPa, and at the angle of $\vartheta = 30°$. This replicates the information given by the sample. Some modifications would need to be made to these properties to fit failure for a triaxial simulation rather than the current plane strain approximation of the test. However, the prelocalization mechanics is not the focus of this simulation: The properties have been chosen only to reach the localization conditions specified by *Wong* [1986]. The predicted force-displacement

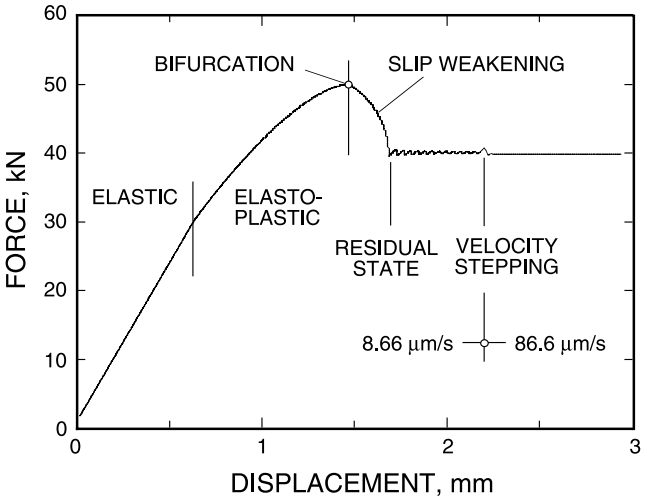

Figure 11. Force displacement response for triaxial compression of San Marcos gabbro (sample G3) predicted by 2-D finite element analysis

curve for the gabbro is shown in Figure 11 and reflects several stages of deformation: elastic, elastoplastic, bifurcation, slip weakening, residual state, and, finally, velocity stepping at residual state.

[42] The initial postlocalization softening (slip weakening regime) is slightly concave downward. This is exactly as predicted from simplified softening law for this problem. Once the cohesion is reduced to zero, some oscillation may be observed in the frictional stress. This is due to the rate- and state-dependent nature of the friction law employed. The viscous damping is not enough to immediately curtail oscillations in the slip speed. Eventually, however, the friction does start to settle to a steady state value. Then, the velocity is increased to 86.6 μm/s to show the effect of rate change on the sample. The sample exhibits the initial increase and final decrease of the friction coefficient characteristic of the friction model. Also, we again see some oscillation in the coefficient of friction, but this is damped out far more quickly at the higher velocity. This unstable/stable slip behavior in the sample is predicted by the model and is analogous to the spring-slider examples discussed, for example, by *Ruina* [1983]. In addition to the slip velocity, slip stability depends on the spring stiffness of the material. Hence a rigid approximation of the model would not be able to predict this behavior.

6. Closure

[43] We have presented a framework for mathematical modeling of slip weakening in an initially intact rock due to shear strain localization along any arbitrary slip plane. The framework includes a closed-form expression for a linear evolution of shear stress with slip up until the full development of a fault, given the stress path on the normal stress-shear stress plane for this fault. The formulation also includes a variable coefficient of friction, which we have implemented into a finite element framework using an embedded strong discontinuity approach. The finite element model may be used not only to analyze rock test data but also to simulate faulting of the Earth's crust on a much larger scale. Work is underway to incorporate dynamic slip instability associated with rupture propagation along fault zones to better understand the influence of tectonic forces and fault properties on the ensuing seismic ground motion.

[44] **Acknowledgments.** We thank D. D. Pollard and J. R. Rice for discussion on the basic issues addressed in this paper, and for providing numerous references relevant to this work. We also thank the three anonymous reviewers for their constructive reviews. We acknowledge the support of the U.S. National Science Foundation, grant CMG-0417521 (Collaborations in Mathematical Geosciences). The first author acknowledges the support of the U.S. Department of Energy grant DE-FG02-03ER15454; the second author acknowledges a research assistantship provided by Sandia National Laboratories, as well as the ARCS Foundation Stanford Graduate Fellowship.

References

Anderson, E. M. (1951), *The Dynamics of Faulting and Dyke Formation with Application to Britain*, Oliver and Boyd, White Plains, N. Y.

Aydin, A., R. I. Borja, and P. Eichnubl (2006), Geological and mathematical framework for failure modes in granular rock, *J. Struct. Geol.*, *28*, 83–98.

Barenblatt, G. I. (1962), The mathematical theory of equilibrium cracks in brittle fracture, *Adv. Appl. Mech.*, *7*, 55–129.

Ben-Zion, Y., and J. R. Rice (1997), Dynamic simulation of slip on a smooth fault in an elastic solid, *J. Geophys. Res.*, *102*, 17,771–17,784.

Bilby, B. A., A. H. Cottrell, and K. H. Swindon (1963), The spread of plastic yield from a notch, *Proc. R. Soc. London, Ser. A*, *272*, 304–314.

Bolt, B. A. (1970), Causes of earthquakes, in *Earthquake Engineering*, edited by R. L. Wiegel, pp. 21–45, Prentice-Hall, Upper Saddle River, N. J.

Borja, R. I. (2000), A finite element model for strain localization analysis of strongly discontinuous fields based on standard Galerkin approximations, *Comput. Methods Appl. Mech. Eng.*, *190*(11–12), 1529–1549.

Borja, R. I. (2002), Finite element simulation of strain localization with large deformation: Capturing strong discontinuity using a Petrov-Galerkin multiscale formulation, *Comput. Methods Appl. Mech. Eng.*, *191*(27–28), 2949–2978.

Borja, R. I. (2004), Computational modeling of deformation bands in granular media, II: Numerical simulations, *Comput. Methods Appl. Mech. Eng.*, *193*(27–29), 2699–2718.

Borja, R. I., and A. Aydin (2004), Computational modeling of deformation bands in granular media, I: Geological and mathematical framework, *Comput. Methods Appl. Mech. Eng.*, *193*(27–29), 2667–2698.

Borja, R. I., and R. A. Regueiro (2001), Strain localization of frictional materials exhibiting displacement jumps, *Comput. Methods Appl. Mech. Eng.*, *190*(20–21), 2555–2580.

Campillo, M., and I. R. Ionescu (1997), Initiation of antiplane shear instability under slip dependent friction, *J. Geophys. Res.*, *102*, 20,363–20,371.

Chester, F. M., and N. G. Higgs (1992), Multi-mechanism friction constitutive model for ultra-fine quartz gouge at hypocentral conditions, *J. Geophys. Res.*, *97*, 1859–1870.

Dieterich, J. H. (1979), Modeling of rock friction: 1. Experimental results and constitutive equations, *J. Geophys. Res.*, *84*, 2161–2168.

Dieterich, J. H., and B. D. Kilgore (1996), Imaging surface contacts: power law contact distributions and contact stresses in quartz, calcite, glass and acrylic plastic, *Tectonophysics*, *256*, 219–239.

Dieterich, J. H., and M. F. Linker (1992), Fault stability under conditions of variable normal stress, *Geophys. Res. Lett.*, *19*(16), 1691–1694.

Dugdale, D. S. (1960), Yielding of steel sheets containing slits, *J. Mech. Phys. Solids*, *8*, 100–104.

Evans, B., J. T. Fredrich, and T.-F. Wong (1990), The brittle-ductile transition in rocks: Recent experimental and theoretical progress, in *The Brittle-Ductile Transition in Rocks*, *Geophys. Monogr. Ser.*, vol. 56, edited by A. G. Duba et al., pp. 1–20, AGU, Washington, D. C.

Guiton, M. L. E., W. Sassi, Y. M. Leroy, and B. D. M. Gauthier (2003), Mechanical constraints on the chronology of fracture activation in folded Devonian sandstone of the western Moroccan Anti-Atlas, *J. Struct. Geol.*, *25*, 1317–1330.

Hadamard, J. (1903), *Lecons sur la Propagation des Ondes*, Herman, Paris.

Hill, R. (1958), A general theory of uniqueness and stability in elastic-plastic solids, *J. Mech. Phys. Solids*, *6*, 236–249.

Ida, Y. (1972), Cohesive force across the tip of a longitudinal shear crack and Griffith's specific surface energy, *J. Geophys. Res.*, *77*, 3796–3805.

Jaeger, J. C., and N. G. W. Cook (1969), *Fundamentals of Rock Mechanics*, CRC Press, Boca Raton, Fla.

Lapusta, N. (2005), Modes of dynamic rupture propagation and rupture front speeds in earthquake models that account for dynamic weakening mechanisms, *Eos Trans. AGU*, *86*(52), Fall Meet. Suppl., Abstract S34A-07.

Lapusta, N., J. R. Rice, Y. Ben-Zion, and G. Zheng (2000), Elastodynamic analysis for slow tectonic loading with spontaneous rupture episodes on faults with rate- and state-dependent friction, *J. Geophys. Res.*, *105*, 23,765–23,789.

Leroy, Y. M., and W. Sassi (2000), A plasticity model for discontinua, in *Aspect of Tectonic Faulting*, edited by F. K. Lehner and J. L. Urai, pp. 77–108, Springer, New York.

Linker, M. F., and J. H. Dieterich (1992), Effects of variable normal stress on rock friction: Observations and constitutive equations, *J. Geophys. Res.*, *97*, 4923–4940.

Mandel, J. (1966), Conditions de stabilité et postulat de Drucker, in *Proceedings IUTAM Symposium on Rheology and Soil Mechanics*, pp. 58–68, Springer, New York.

Matsuoka, H., and T. Nakai (1974), Stress-deformation and strength characteristics of soil under three different principal stresses, *Proc. Jpn. Soc. Civ. Eng.*, *232*, 59–70.

Mitchell, J. K. (1993), *Fundamentals of Soil Behavior*, 2nd ed., John Wiley, Hoboken, N. J.

Ohnaka, M., M. Akatsu, H. Mochizuki, A. Odedra, F. Tagashira, and Y. Yamamoto (1997), A constitutive law for the shear failure of rock under lithospheric conditions, *Tectonophysics*, *277*, 1–27.

Okubo, P. G., and J. H. Dieterich (1984), Effects of physical fault properties on frictional instabilities produced on simulated faults, *J. Geophys. Res.*, *89*, 5817–5827.

Palmer, A. C., and J. R. Rice (1973), The growth of slip surfaces in the progressive failure of overconsolidated clay, *Proc. R. Soc. London, Ser. A*, *332*, 527–548.

Paterson, M. S. (1990), Rock deformation experimentation, in *The Brittle-Ductile Transition in Rocks*, *Geophys. Monogr. Ser.*, vol. 56, edited by A. G. Duba et al., pp. 187–194, AGU, Washington, D. C.

Regueiro, R. A., and R. I. Borja (2001), Plane strain finite element analysis of pressure-sensitive plasticity with strong discontinuity, *Int. J. Solids Struct.*, *38*(21), 3647–3672.

Rice, J. R. (1980), The mechanics of earthquake rupture, in *Physics of the Earth's Interior*, edited by A. M. Dziewonski and E. Boschi, pp. 555–649, Elsevier, New York.

Rice, J. R. (2006), Heating and weakening of faults during earthquake slip, *J. Geophys. Res.*, *111*, B05311, doi:10.1029/2005JB004006.

Rice, J. R., and Y. Ben-Zion (1996), Slip complexity in earthquake fault models, *Proc. Natl. Acad. Sci. U.S.A.*, *93*, 3811–3818.

Rice, J. R., and M. Cocco (2007), Seismic fault rheology and earthquake dynamics, in *The Dynamics of Fault Zones, Dahlem Workshop Rep. 95*, edited by M. R. Handy, MIT Press, Cambridge, Mass., in press.

Rice, J. R., and A. L. Ruina (1983), Stability of steady frictional slipping, *J. Appl. Mech.*, *50*, 343–349.

Rudnicki, J. W. (1980), Fracture mechanics applied to the Earth's crust, *Annu. Rev. Earth Planet. Sci.*, *8*, 489–525.

Rudnicki, J. W., and J. R. Rice (1975), Conditions for the localization of deformation in pressure-sensitive dilatant materials, *J. Mech. Phys. Solids*, *23*, 371–394.

Ruina, A. L. (1983), Slip instability and state variable friction laws, *J. Geophys. Res.*, *88*, 10,359–10,370.

Rummel, F., H. J. Alheid, and C. Frohn (1978), Dilatancy and fracture-induced velocity changes in rock and their relation to frictional sliding, *Pure Appl. Geophys.*, *116*, 743–764.

Scholz, C. H. (1990), *The Mechanics of Earthquakes and Faulting*, Cambridge Univ. Press, New York.

Sibson, R. H. (1986), Earthquakes and rock deformation in crustal fault zones, *Annu. Rev. Earth Planet. Sci.*, *14*, 149–175.

Sibson, R. H. (1989), Earthquake faulting as a structural process, *J. Struct. Geol.*, *11*(1/2), 1–14.

Stakgold, I. (1998), *Green's Functions and Boundary Value Problems*, 2nd ed., John Wiley, Hoboken, N. J.

Thomas, T. Y. (1961), *Plastic Flow and Fracture of Solids*, Elsevier, New York.

Uenishi, K., and J. R. Rice (2003), Universal nucleation length for slip-weakening rupture instability under nonuniform fault loading, *J. Geophys. Res.*, *108*(B1), 2042, doi:10.1029/2001JB001681.

Wawersik, W. R., and W. F. Brace (1971), Post-failure behavior of a granite and a diabase, *Rock Mech.*, *3*, 61–85.

Wawersik, W. R., and C. Fairhusrt (1970), A study of brittle rock fracture in laboratory compression experiments, *Int. J. Rock Mech. Min. Sci.*, *7*, 561–575.

Wong, T.-F. (1982), Shear fracture energy of westerly granite from post-failure behavior, *J. Geophys. Res.*, *87*, 990–1000.

Wong, T.-F. (1986), On the normal stress dependence of the shear fracture energy, in *Earthquake Source Mechanics*, *Geophys. Monogr. Ser.*, vol. 37, edited by S. Das, J. Boatwright, and C. H. Scholz, pp. 1–11, AGU, Washington D. C.

R. I. Borja and C. D. Foster, Department of Civil and Environmental Engineering, Stanford University, Stanford, CA 94305, USA. (borja@stanford.edu)